Supplementary Data

Experimental Methods

Western blot after laser capture microdissection

The protein content was measured with Western blot (WB) (5,6). To prepare frozen tissue sections, we collected hippocampi from postnatal 7-day-old Sprague-Dawley rats (Charles River, Pittsburgh), froze them in a cryopreservative solution matrix (1), and sliced them into frozen sections at 100 μm thickness. Every three frozen slices were transferred to a normal glass slide, uncovered, and followed by the hematoxylin and eosin stain (1) (but without treating with xylene) to reveal the anatomy of organotypic hippocampal slice culture (OHSC). The pyramidal cells in the subfield of OHSC (Fig. 4A) were cut out by laser capture microdissection (LCM) (1) using an Arcturus PixCell IIe LCM device (Molecular Devices, LLC).

To collect enough samples, pyramidal cells of CA1 or CA3 were collected from $\sim$50 frozen sections to ensure $\sim$10 μg of total protein that could be extracted. The LCM harvested tissue was lysed in 10 μl RIPA buffer with phenylmethanesulfonyl fluoride (PMSF) from Cell Signaling Technology, sonicated on ice with 10 rounds of cycles (15 s pulse on and 1 min pulse off) at 15% power with a Fisher Scientific 550 sonic dismembrator, and then loaded to a 12% polyacrylamide gel for separation. Primary antibodies and secondary antibodies were applied to detect complex I, SOD2, thioredoxin 2, and α-tubulin (used as internal control) by following the WB protocol from Bio-Rad Laboratories, Inc.

Following antibodies were used here: rabbit anti-ND4L (sc-20665) from Santa Cruz Biotechnology, Inc.; rabbit anti-SOD2 (ab13533) and rabbit anti-Trx2 (ab185544) from Abcam, Inc.; and mouse anti-α-tubulin (No. 3873), anti-rabbit IgG, HRP-linked Antibody (No. 7074), and anti-mouse IgG, HRP-linked Antibody (No. 7076) from Cell Signaling Technology. Chemiluminescence was detected by using SignalFire™ Elite ECL Reagent (No. 12757; Cell Signaling Technology). Band intensity ratio was used to quantify the protein content corresponding to the internal standard, α-tubulin. It is calculated using the equation shown below.

$$\mathrm{BIR} = \frac{\mathrm{BI}_{\mathrm{protein}}}{\mathrm{BI}_{\alpha-\mathrm{tubulin}}}. \tag{S1}$$

Quantitative analysis of the protein content from OHSCs with immunofluorescence

OHSC was first fixed with 4% paraformaldehyde solution for 5 min, then permeabilized with 1% Triton X-100 phosphate-buffered saline (PBS) solution at 4°C for 18 h, blocked with 20% bovine serum albumin (BSA) for 3 h at room temperature (RT), then incubated with the primary antibody at 4° overnight, followed by incubation with the secondary antibody at RT for 4 h. PBS with 5% BSA was used to rinse. Well-prepared OHSCs on glass slides were imaged with a 63$\times$oil immersion objective lens. Images from CA1 and CA3 within one OHSC were acquired with the same imaging parameters and processed by ImageJ with incorporated multiplugins.

Following antibodies were used: rabbit anti-ND4L (sc-20665), rabbit anti-TrxR2 (sc-67127), and rabbit anti-TrxR1 (sc-20147) from Santa Cruz Biotechnology, Inc.; rabbit anti-SOD2 (ab13533), rabbit anti-Prx3 (ab73349), rabbit anti-Prx2 (ab109367), rabbit anti-Grx2 (ab191292), rabbit anti-Gpx1 (ab108427), rabbit anti-GR (ab16801), and rabbit anti-Trx2 (ab185544) from Abcam, Inc.; rabbit anti-Prx1 (PA3-750) and goat anti-rabbit with Alexa Fluor® 488 (A-11008) from Thermo Fisher; rabbit anti-Trx 1 (No. 2429) and mouse anti-α-tubulin (No. 3873) from Cell Signaling Technology; goat anti-rabbit with CF™ 568 (No. 20103-1) from Biotium; goat anti-mouse IgG with CF 488A (SAB4600387; Sigma-Aldrich, USA); and rabbit anti-Prx5 (No. 17724-1-AP) from ProteinTech.

Mitochondrial proteins (*i.e.*, ND4L, SOD2, Trx2, TrxR2, Prx3, Prx5, and Grx2) were immunostained and imaged at Exi: 488 nm, Emi: 500–530 nm, while mitochondria were labeled with MitoTracker®deep red FM (No. M22426; Thermo Fisher Scientific) and imaged at Exi: 633 nm, Emi: 660–680 nm. MitoTracker was applied to live tissue before fixation for 30 min at 37°C. The fluorescence intensity of mitochondrial protein is counted only from the mitochondria area of pyramidal cell layer and normalized to that of MitoTracker (see Supplementary Fig. S5 for more details).

Cytosolic proteins (*i.e.*, Trx1, TrxR1, Prx1, and Prx2) were immunostained and imaged at Exi: 561 nm, Emi: 575–595 nm. α-Tubulin was immunostained and imaged at Exi: 488 nm, Emi: 500–530 nm. The procedure for extracting the fluorescence intensity of cytosolic protein and α-tubulin is presented in Supplementary Figure S5, and α-tubulin was used as an internal standard for cytosolic proteins. Fluorescence ratio was used to quantify the protein content corresponding to the internal standard. Mitochondrial protein and cytosolic protein were calculated using Equations (S2) and (S3), respectively.

$$\mathrm{FR} = \frac{\mathrm{F}_{\mathrm{mito\ protein}}}{\mathrm{F}_{\mathrm{MitoTracker}}} \tag{S2}$$

$$\mathrm{FR} = \frac{\mathrm{F}_{\mathrm{cyto\ protein}}}{\mathrm{F}_{\alpha-\mathrm{tubulin}}}. \tag{S3}$$

Overexpression of hTrx1 and characterization

The plasmid coding for recombinant human Trx1 (hTrx1) was obtained from Addgene (FLAG-TRX; No. 21615) (3). It was coexpressed with the roGFP2 probe for H_2O_2 or glutathione (GSH) by gene gun. To verify the expression of hTrx1, OHSCs were fixed and stained by following the protocols depicted in the previous section. A recombinant protein with a polypeptide protein tag and thioredoxin (FLAG-TRX) was stained with primary antibody that is selective to hTrx1, rabbit anti-hTrx1 antibody (No. 2285; Cell Signaling, Tech.), and secondary antibody, goat anti-rabbit with CFTM568 (No. 20103-1; Biotium). The roGFP2 was stained with mouse anti-green fluorescent protein (GFP) (11814460001; Roche) (2) and secondary antibody, goat anti-mouse IgG, with CF 488A (SAB4600387; Sigma-Aldrich). To verify the upregulation of Trx1, the sum of hTrx1, and rat Trx1 (rTrx1), we adopted the procedures above, except rabbit anti-Trx1 (No. 2429; Cell Signaling, Tech.) was used as primary antibody for hTrx1 and rTrx1.

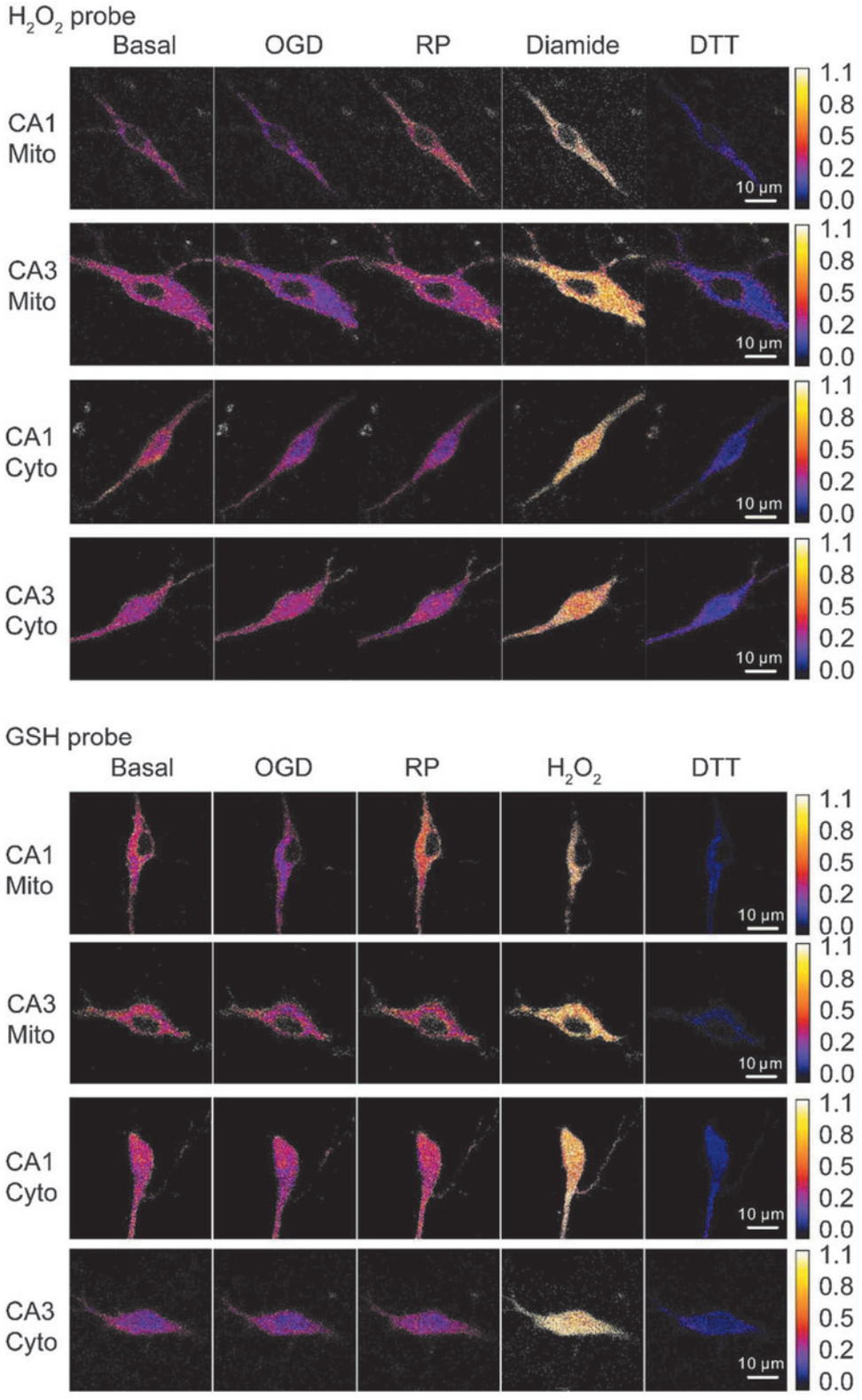

SUPPLEMENTARY FIG. S1. Ratiometric images of pyramidal cells expressing roGFP2-Orp1 or Grx1-roGFP2 (related to Fig. 1). Ratiometric images of H_2O_2 probe (*top*) or GSH probe (*bottom*) expressed in mitochondria (Mito) or cytoplasm (Cyto) of pyramidal cells in CA1 or CA3 are acquired according to the protocol described in the Experimental Methods section in Supplementary Data. The value of $R_{405/488}$ ($0 < R_{405/488} < 1$), indicated in the calibration *color bar*, reflects the oxidation degree of the probe. Cells are fully oxidized by diamide (shown in *brightest color*, $R_{405/488} = 1$) and fully reduced by DTT (shown in *darkest purple*, $R_{405/488} \approx 0.25$ for H_2O_2 probe and $R_{405/488} \approx 0.18$ for GSH probe). Noticeable change in oxidation degree (reflected by *color*) is found in mitochondria, but not in cytoplasm during the OGD-RP experiment. GSH, glutathione.

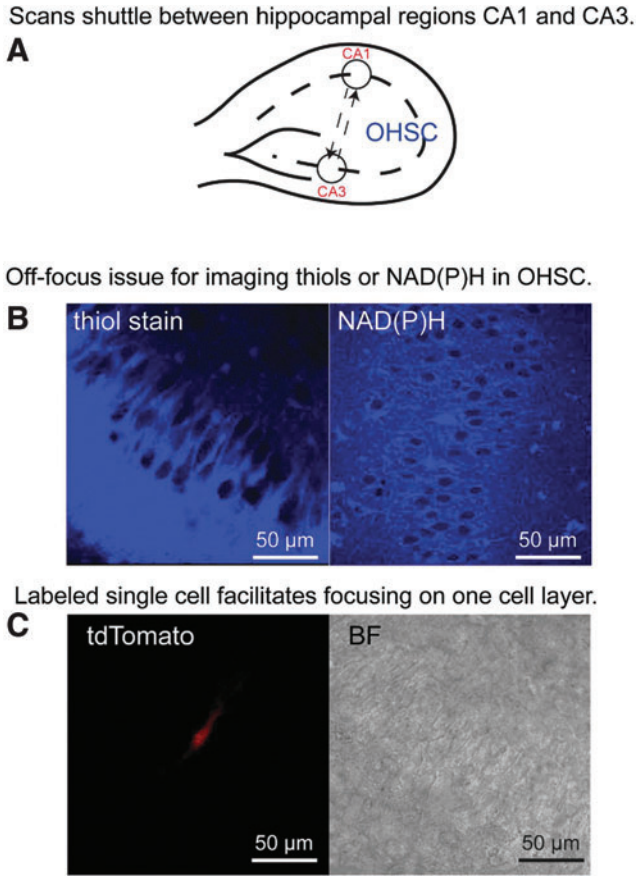

SUPPLEMENTARY FIG. S2. Optimization of thiols/NAD(P)H imaging (related to Fig. 3 and Supplementary Fig. S3). (A) Scans shuttle between CA1 and CA3 to allow fluorescence signals from two areas to be acquired at the same time frame. This enables direct comparison between CA1 and CA3 without calibration by using internal or external standards. **(B)** The ATF function was applied on the Leica confocal microscope aiming to limit the error in the Z-direction within ±1 μm over time. The algorithm of this function is to find the largest FA and highest FI. Its application depends on the different FA and FI varying in different depths. However, the fluorescence from NAD(P)H and thiols in OHSCs presents as honeycomb patterns, which do not show significant differences of FA and FI at various depths, leading to the failure of the ATF function. **(C)** tdTomato was introduced to a single pyramidal cell. ATF can easily maintain the focus on the equatorial plane (where largest FA and highest FI were found) of this labeled cell with *Z*-axis shift <1 μm. ATF, autofocus; FA, fluorescent area; FI, fluorescence intensity; OHSC, organotypic hippocampal slice culture.

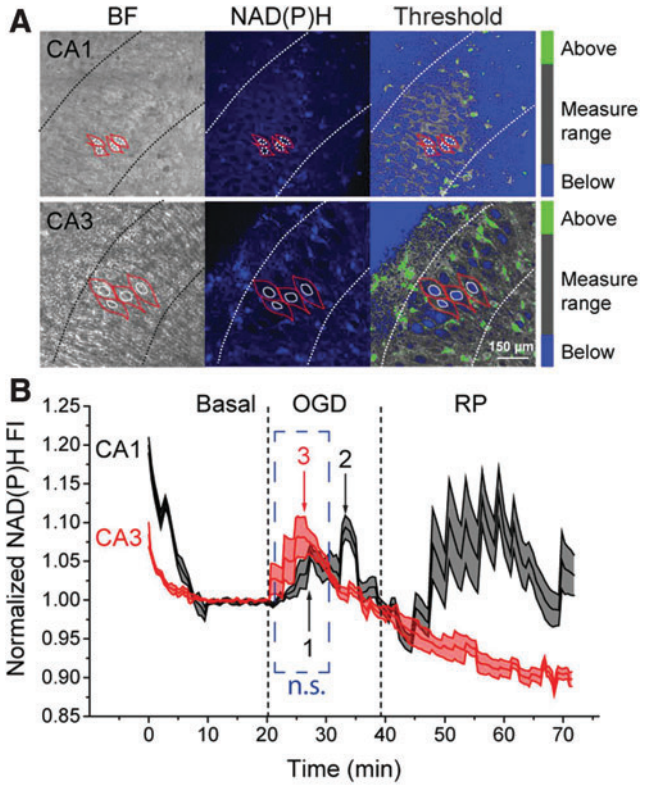

SUPPLEMENTARY FIG. S3. A larger change in NAD(P)H is found in CA1 *versus* CA3 (related to Fig. 1). (A) Bright-field image (*left*), two-photon image (ex 740 nm, em 580–630 nm) from the pyramidal cell layer (*middle*), and threshold image (*right*). The area of interest is shown in *gray* (above in *green*, below in *blue*). Several cells are outlined with *red closed lines* and nuclei are encircled by *white closed lines*. Nuclei have much lower NAD(P)H content than the rest of the cell according to the fluorescence intensity. The pyramidal cells are larger in size in CA3 (*bottom*) than in CA1 (*top*). **(B)** The normalized fluorescence intensity of NAD(P)H (mean ± SEM, $n = 6$ slices) changes during OGD-RP. FI is normalized to the stable basal value. The first peak (labeled 1) in CA1 is not significantly different from the peak (labeled 3) in CA3. During RP, NAD(P)H in CA1 oscillates around a notably higher level than in CA3, and NAD(P)H keeps dropping during RP in CA3. See the Peak Analysis section in Supplementary Data for more details.

Cell death assay: propidium iodide stain and imaging

OHSCs treated with oxygen–glucose deprivation (OGD)–reperfusion (RP) were stained with 7 μM propidium iodide (PI) overnight (7). We imaged PI-stained OHSC with 561 nm excitation and 600–640 nm emission (Fig. 7). The cell death percentage in a particular area of OHSC was calculated as below:

$$Death\% = \frac{(I_{sample} - I_{negative})}{(I_{positive} - I_{negative})} \times 100\%. \qquad (S4)$$

I_{sample}, $I_{positive}$, and $I_{negative}$ are fluorescence intensity from the tested OHSC, the positive control, and the negative control, respectively. In this study, we use 100% methanol-treated OHSC as the positive control (assuming 100% cell death) and healthy OHSC as the negative control (assuming 0% cell death).

Linear regression

Linear data segments were analyzed in the statistical software, R, to extract parameters, mean and slope of the lines, with linear regression. In Figure 1E and F, the traces were divided into several portions with a singular linear trend. The linear parameters, mean and slope, were compared according to two subcategories, OGD-RP time period (basal *vs.* OGD *vs.* RP; one-way ANOVA) and tissue subfield (CA1 *vs.* CA3; *t*-test with bootstrap). In Figure 2B and D, the data in I

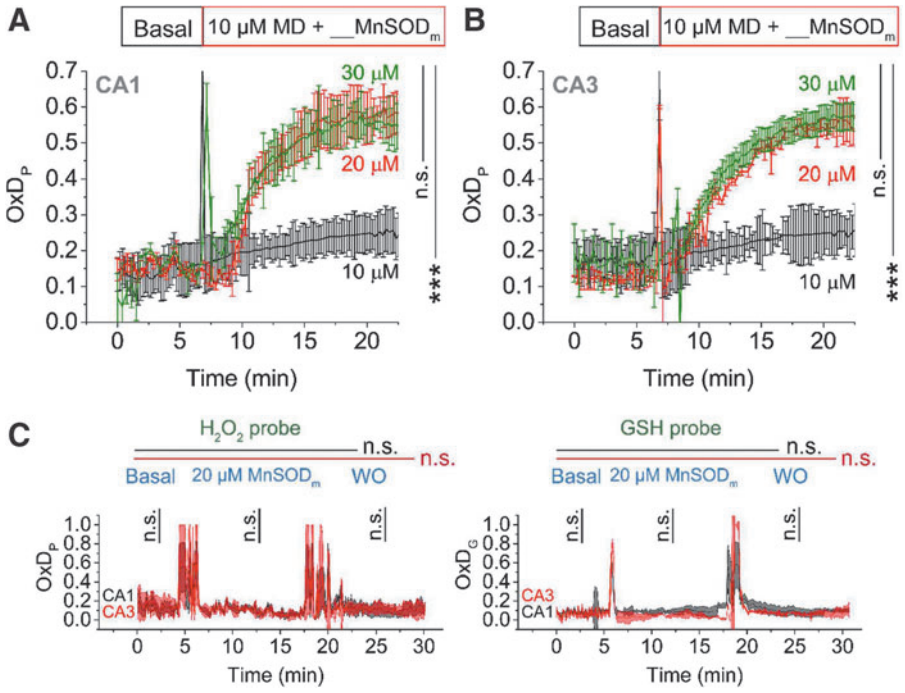

SUPPLEMENTARY FIG. S4. The minimum concentration of $MnSOD_m$ sufficient for maximal generation of peroxide in OHSCs ($[MnSOD_m]_{max}$) is 20 μ*M* and $MnSOD_m$ alone has no effect on OxDs (related to Fig. 2). (A, B) An OHSC is first superfused with ACSF solution (basal), then with 10 μ*M* menadione+MnSOD mimic ($MnSOD_m$). Three different concentrations of $MnSOD_m$ were used: 10, 20, and 30 μ*M*. Sharp changes of OxD_P were found from 10 to 20/30 μ*M* $MnSOD_m$ (marked by *long vertical line*). No further change from 20 to 30 μ*M* $MnSOD_m$ (marked by *short vertical line*) indicates that 20 μ*M* is sufficient. The steady OxD_P values can be acquired from the last 5 min of MD+$MnSOD_m$. All traces are mean ± SEM ($n = 6$ repeats). Curves during MD+$MnSOD_m$ superfusion were fitted by the first-order exponential equation (see Nonlinear Regression to the First-Order Exponential Equation section in Supplementary Data for more details). Parameters were analyzed with a *t*-test with bootstrap or one-way ANOVA with *post hoc* test (n.s, no significant difference, $p > 0.05$, ***$p < 0.001$). **(C)** OHSC is treated with ACSF/20 μ*M* $MnSOD_m$/ACSF for 5/15/15 min. Each trace is mean ± SEM, $n = 6$ repeats. No changes of OxD_P and OxD_G are found through basal/20 μ*M* $MnSOD_m$/WO (indicated by *horizontal lines*, *black* for CA1, *red* for CA3) or between CA1 and CA3 (indicated by *vertical lines*). One-way ANOVA test/*t*-test result is noted as n.s. if no significant difference, $p > 0.05$, is found.

to III with linear trends were fitted and linear parameters were compared according to two subcategories, treat period (basal *vs.* 10 μ*M* MD *vs.* washout [WO]; one-way ANOVA) and tissue subfield (CA1 *vs.* CA3; *t*-test with bootstrap). The same criteria (no significant difference, n.s., $p > 0.05$, *$p < 0.05$, **$p < 0.01$, ***$p < 0.001$) were used to present the analysis result.

Peak analysis

The peaks in Supplementary Figure S3 were analyzed in an open-source statistical software, R (www.r-project.org), to obtain four parameters, peak altitude, ascending slope, descending slope, and the emerging time of the peak from the onset of OGD. All of the peak parameters from different peaks were compared with a *t*-test with bootstrap (no significant difference, n.s., $p > 0.05$, *$p < 0.05$, **$p < 0.01$, ***$p < 0.001$).

Nonlinear regression to the first-order exponential equation

As shown in Figure 1C, the enzymatic subunits of the H_2O_2 probe, Orp1 (left), and of the GSH probe, Grx1 (right), catalyze the coupling of probes with their relative redox couples. The rate equations of OxD_P and OxD_G are derived as below according to Figure 1C:

H_2O_2 probe

$$[Orp1]_T \frac{dOxD_P}{dt} = \frac{d[Orp1]_{Ox}}{dt} = k_1[H_2O_2][Orp1]_{Red} - k_2[Trx]_{Red}[Orp1]_{Ox} \quad \text{(S5)}$$

$$[Orp1]_T = [Orp1]_{Red} + [Orp1]_{Ox} \quad \text{(S6)}$$

$$OxD_P = \frac{[Orp1]_{Ox}}{[Orp1]_T} \quad \text{(S7)}$$

$$\frac{dOxD_P}{dt} = k_1[H_2O_2] - \left(k_1[H_2O_2] + k_2[Trx]_{Red}\right)OxD_P \quad \text{(S8)}$$

in which $[Orp1]_T$, $[Orp1]_{Ox}$, and $[Orp1]_{Red}$ are the concentration of the total form, oxidized form, and reduced form of roGFP2-Orp1, respectively. $[H_2O_2]$ is the concentration of H_2O_2. $[Trx]_{Red}$ is the concentration of the reduced form of Trx. H_2O_2 and Trx_{red} are all first order in their reactions with Orp1 at different redox forms in our H_2O_2 probe, roGFP2-Orp1 (4,8).

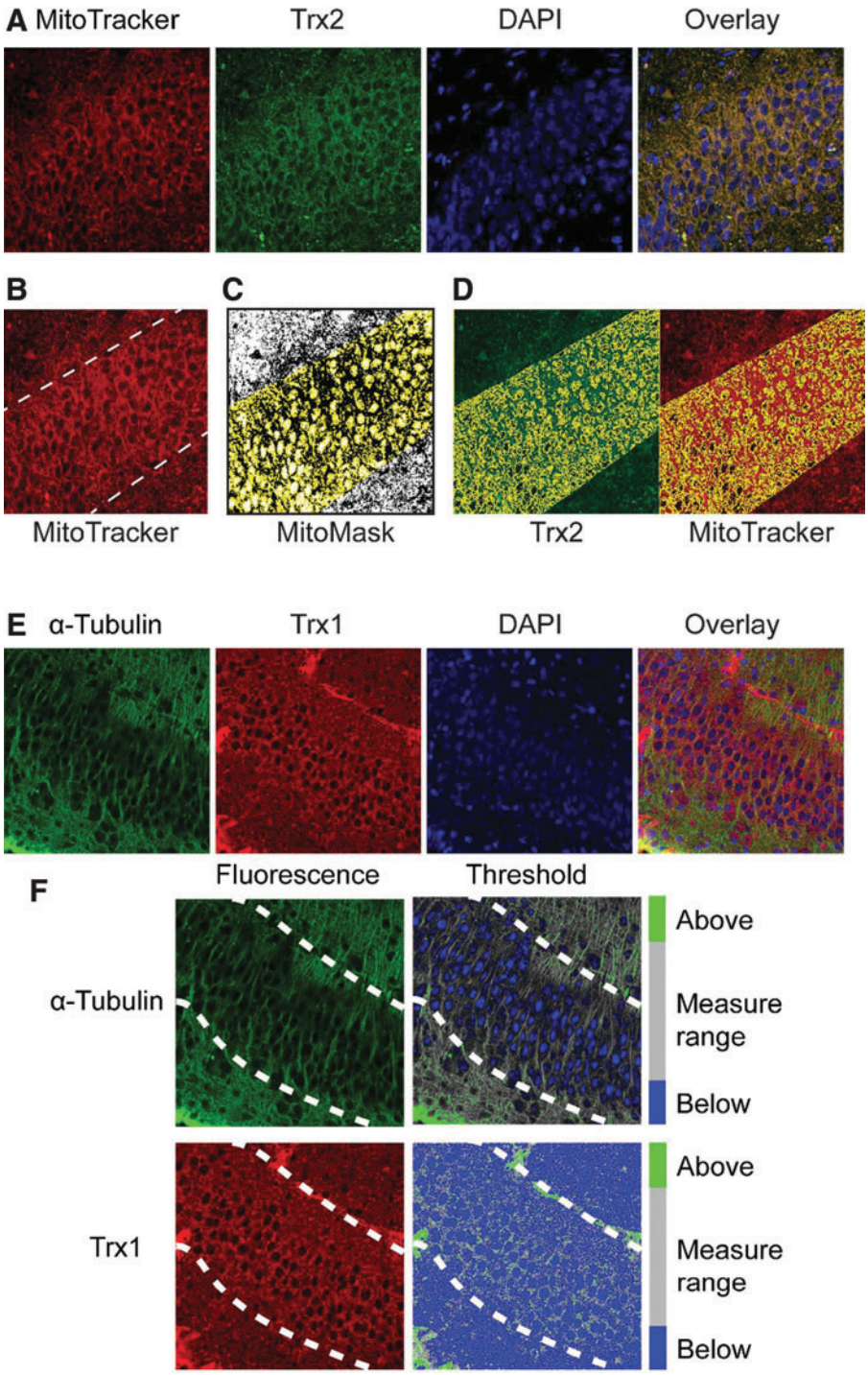

SUPPLEMENTARY FIG. S5. Quantitative measurement of a target protein in OHSCs by referring to the internal control *via* immunofluorescence (related to Fig. 4). (A–D) Examples from Trx2 demonstrate the quantitative measurement of a mitochondrial protein referenced to MitoTracker. **(A)** Representative fluorescence images from subfield CA1 of a triple stained OHSC. From *left* to *right*, mitochondria are stained with MitoTracker, shown in *red*; Trx2 is immunostained, shown in *green*; nuclei are counterstained with DAPI, shown in *blue*; the final image is the overlay of the former three. **(B–D)** Create a mask of mitochondria by using MitoTracker for measuring the mitochondrial protein such as Trx2. **(B)** The mitochondria in OHSC are stained by MitoTracker. The pyramidal cell layer (in CA1 here) is indicated within the *white dash lines*. **(C)** Mitochondria are shown in *black* after setting the threshold of image in **(B)**. The *yellow* selection is created in ImageJ and indicates the mitochondria of the pyramidal cell layer. **(D)** Fluorescence intensity from Trx2 and MitoTracker in the *yellow* selection is acquired **(C)**. The intensity from Trx2 was normalized to that of MitoTracker [see Eq. (S2)]. **(E, F)** Examples from Trx1 demonstrate the quantitative measurement of a cytosolic protein referring to α-tubulin. **(E)** Representative fluorescence images from subfield CA1 of a triple stain. From *left* to *right*, α-tubulin is immunostained, shown in *green*; Trx1 is immunostained, shown in *red*; and nuclei are counterstained with DAPI, shown in *blue*; the final image is the overlay of all three. **(F)** α-tubulin (*top*) and Trx1 (*bottom*) are displayed. Fluorescence images (*left column*) were processed into the images with thresholds in the *right column* (the area within threshold is shown in *gray*, areas of above and below threshold are in *green* and *blue*, respectively). The ROI is outlined to only include the pyramidal cells in OHSC (*white dashed line*). Only pixels within the threshold in the ROI are counted. The fluorescence intensity of Trx1 was normalized to that of α-tubulin [see Eq. (S3)]. ROI, region of interest.

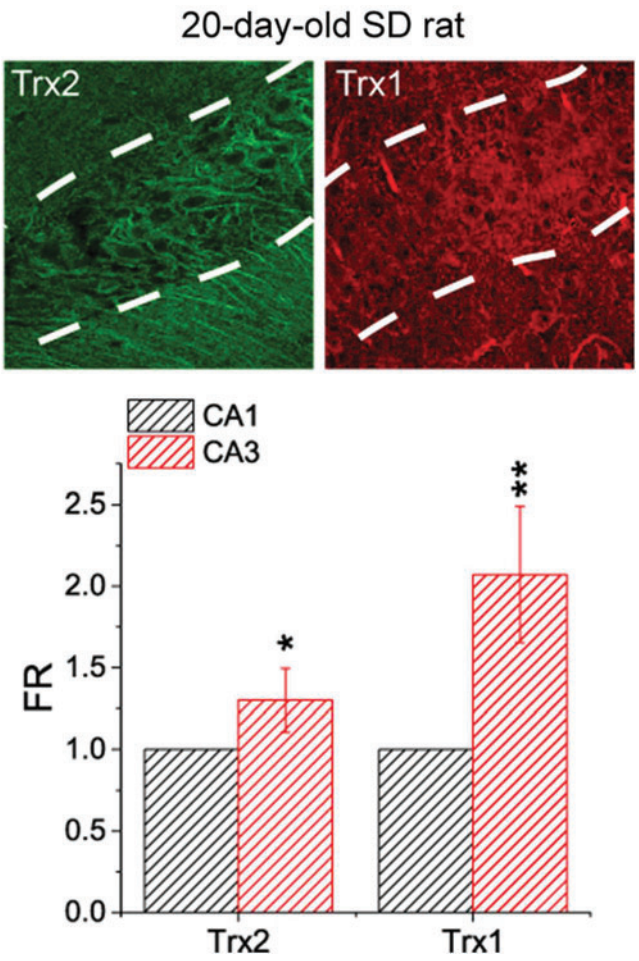

SUPPLEMENTARY FIG. S6. Relative Trx levels in CA1 *versus* CA3 in 20-day-old Sprague-Dawley rat (related to Fig. 4). Data are represented as mean ± SEM, $n = 8$ slices, $*p < 0.05$, $**p < 0.01$. In a 20-day-old rat, Trx2 and Trx1 are found significantly higher in CA3, similar to that found in a 7-day-old rat.

GSH probe

$$[Grx1]_T \frac{dOxD_G}{dt} = \frac{d[Grx1]_{Ox}}{dt} = k_1'[GSSG][Grx1]_{Red} - k_2'[GSH][Grx1]_{Ox} \quad \text{(S9)}$$

$$[Grx1]_T = [Grx1]_{Red} + [Grx1]_{Ox} \quad \text{(S10)}$$

$$OxD_G = \frac{[Grx1]_{Ox}}{[Grx1]_T} \quad \text{(S11)}$$

$$\frac{dOxD_G}{dt} = k_1'[GSSG] - \left(k_1'[GSSG] + k_2'[GSH]\right) OxD_G \quad \text{(S12)}$$

in which $[Grx1]_T$, $[Grx1]_{Ox}$, and $[Grx1]_{Red}$ are the concentration of total forms, oxidized form, and reduced form of Grx1-roGFP2, respectively. $[GSH]$ and $[GSSG]$ are the concentration of GSH and GSSG, respectively. GSH and GSSG are all first order in their reactions with Grx1 at different redox status in our GSH probe, Grx1-roGFP2 (9).

The pseudo first-order reaction model

$$\frac{dx}{dt} = A - kx \quad \text{(S13)}$$

$$x = \frac{A}{k} - \left(\frac{A}{k} - x_0\right) e^{-kt} \quad \text{(S14)}$$

in which A is a constant, k is a reaction rate constant for this pseudo first order, and x is a parameter that changes in a first-order dynamic mechanism.

If we organize Equation (S8) for H_2O_2 probe and Equation (S12) for GSH probe into the form of Equations (S13) and (S14), we get the variables x, A, k, and x_0 for Equation (S14) specified as OxD_P, $k_1[H_2O_2]$, $k_1[H_2O_2]+k_2[Trx]_{Red}$, and OxD_{0P} for the peroxide probe and OxD_G, $k_1'[GSSG]$, $k_1'[GSSG]+k_2'[GSH]$, and OxD_{0G} for the GSH probe. The nonlinear regression was coded and operated in MATLAB (version R2014b; The MathWorks, Inc.). *t*-Test with bootstrap and one-way ANOVA were applied to these fitted parameters in open-source statistical software, R (www.r-project.org) and MATLAB (no significant difference, n.s., $p > 0.05$, $*p < 0.05$, $**p < 0.01$, $***p < 0.001$).

References

1. Espina V, Wulfkuhle JD, Calvert VS, VanMeter A, Zhou W, Coukos G, Geho DH, Petricoin EF, and Liotta LA. Laser-capture microdissection. *Nat Protoc* 1: 586–603, 2006.
2. Kasozi D, Mohring F, Rahlfs S, Meyer AJ, and Becker K. Real-time imaging of the intracellular glutathione redox rotential in the malaria parasite *Plasmodium falciparum*. *PLoS Pathog* 9: e1003782, 2013.
3. Liu H, Nishitoh H, Ichijo H, and Kyriakis JM. Activation of apoptosis signal-regulating kinase 1 (ASK1) by tumor necrosis factor receptor-associated factor 2 requires prior dissociation of the ASK1 inhibitor thioredoxin. *Mol Cell Biol* 20: 2198–2208, 2000.
4. Ma L-H, Takanishi CL, and Wood MJ. Molecular mechanism of oxidative stress perception by the Orp1 protein. *J Biol Chem* 282: 31429–31436, 2007.
5. Martinet W, Abbeloos V, Van Acker N, De Meyer GRY, Herman AG, and Kockx MM. Western blot analysis of a limited number of cells: a valuable adjunct to proteome analysis of paraffin wax-embedded, alcohol-fixed tissue after laser capture microdissection. *J Pathol* 202: 382–388, 2004.
6. Ornstein DK, Gillespie JW, Paweletz CP, Duray PH, Herring J, Vocke CD, Topalian SL, Bostwick DG, Linehan WM, Petricoin EF, and Emmert-Buck MR. Proteomic analysis of laser capture microdissected human prostate cancer and *in vitro* prostate cell lines. *Electrophoresis* 21: 2235–2242, 2000.
7. Riccardi C and Nicoletti I. Analysis of apoptosis by propidium iodide staining and flow cytometry. *Nat Protoc* 1: 1458–1461, 2006.
8. Stone JR and Yang S. Hydrogen peroxide: a signaling messenger. *Antioxid Redox Signal* 8: 243–270, 2006.
9. Xiao R, Lundström-Ljung J, Holmgren A, and Gilbert HF. Catalysis of thiol/disulfide exchange: glutaredoxin 1 and protein-disulfide isomerase use different mechanisms to enhance oxidase and reductase activities. *J Biol Chem* 280: 21099–21106, 2005.

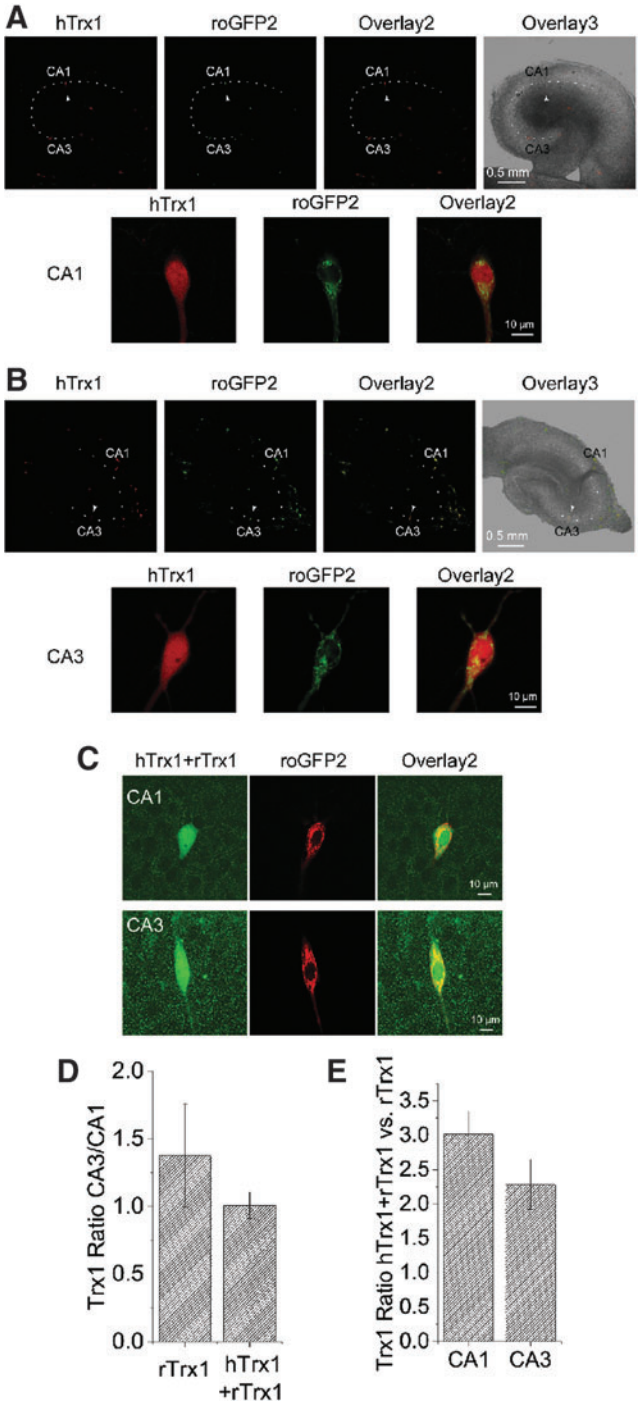

SUPPLEMENTARY FIG. S7. Overexpression of hTrx1 in single cells in OHSCs by gene gun (related to Figs. 4–6). **(A, B)** (*Top*) Representative fluorescence images of immunostained OHSCs. Cells expressing hTrx1 and mitochondrial roGFP2 probe (Mito-Grx1-roGFP2 here) are randomly distributed in OHSCs. hTrx1 and Mito-Grx1-roGFP2 are stained and shown in *red* and *green*, respectively. The pyramidal cell layer is indicated by the *white dash line* and one pyramidal cell is indicated by a *white arrow*. CA1 and CA3 are marked. From *left* to *right*, image of hTrx1, roGFP2, overlay of hTrx1 and roGFP2, and overlay of the former and BF; (*Bottom*) pyramidal cell noted in (*top*) is imaged at a larger magnification. From *left* to *right*, image of hTrx1, roGFP2, and overlay of the former two. **(C)** Both hTrx1 and rTrx1 are stained with the same, nonspecies-specific primary antibody. From *left* to *right*, image of Trx1, image of roGFP2, and overlay of the former two; **(D)** *Left bar*, control, rTrx1 is higher in CA3 than CA1 ($n = 5$); *right bar*, transfected cells, hTrx1+rTrx1: CA1 and CA3 pyramidal cells show no difference in total Trx1 following transfection. **(E)** Quantitative estimate of transfection effectiveness. Ratio of hTrx1+rTrx1 over rTrx1 in each region's pyramidal cells, $n = 5$ repeats. BF, bright-field; hTrx1, human Trx1.

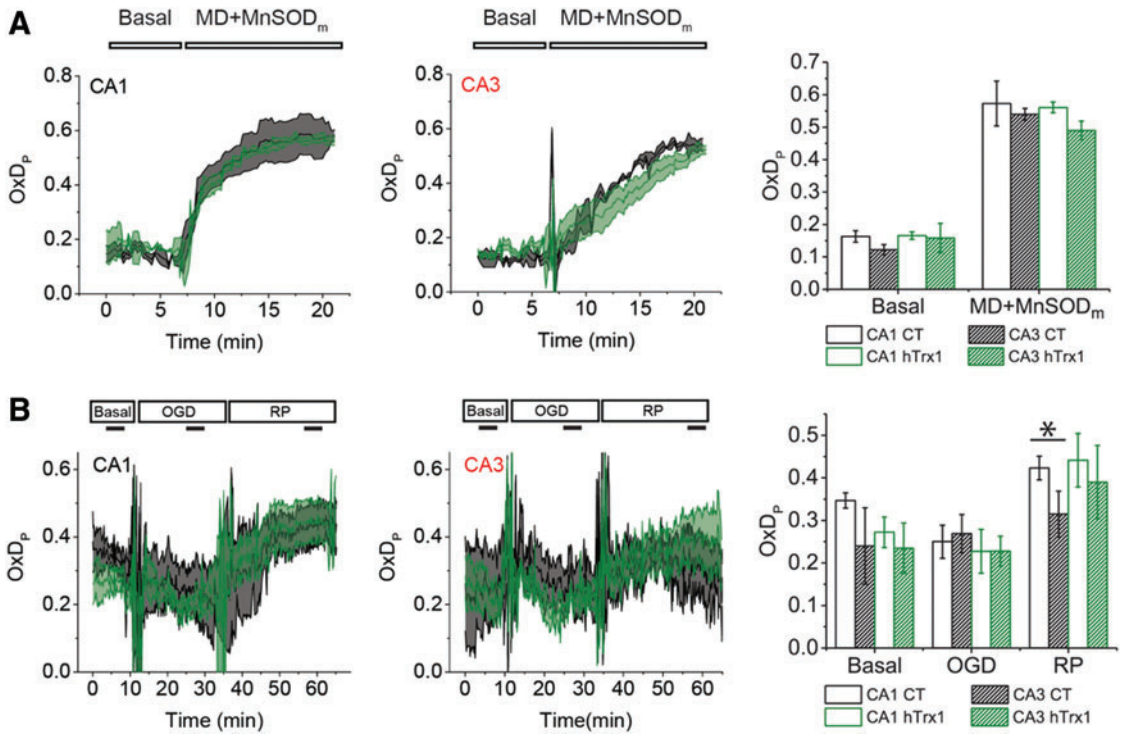

SUPPLEMENTARY FIG. S8. Overexpression of hTrx1 does not alter the mitochondrial H_2O_2 system significantly (related to Figs. 4–6). **(A)** Tissue is superfused with ASCF in basal condition for ~8 min, then with 10 μM MD +20 μM $MnSOD_m$ for 15 min. **(B)** Tissue is treated with 10/20/30 min basal/OGD/RP. In **(A, B)**, data are presented as mean ± SEM ($n = 6$ OHSCs). CT, control data from normal tissue in *gray*. hTrx1, data from hTrx1-overexpressing tissue, in *green*. (*Left*) OxD_P data from CA1 pyramidal cells. (*Middle*) OxD_P data from CA3 pyramidal cells. (*Right*) Data from 5 min of each period before transient are plotted. Student's *t*-test was used for the comparisons of CA1 *versus* CA3 and CT *versus* hTrx1 (no symbol for no significant difference, $*p < 0.05$).

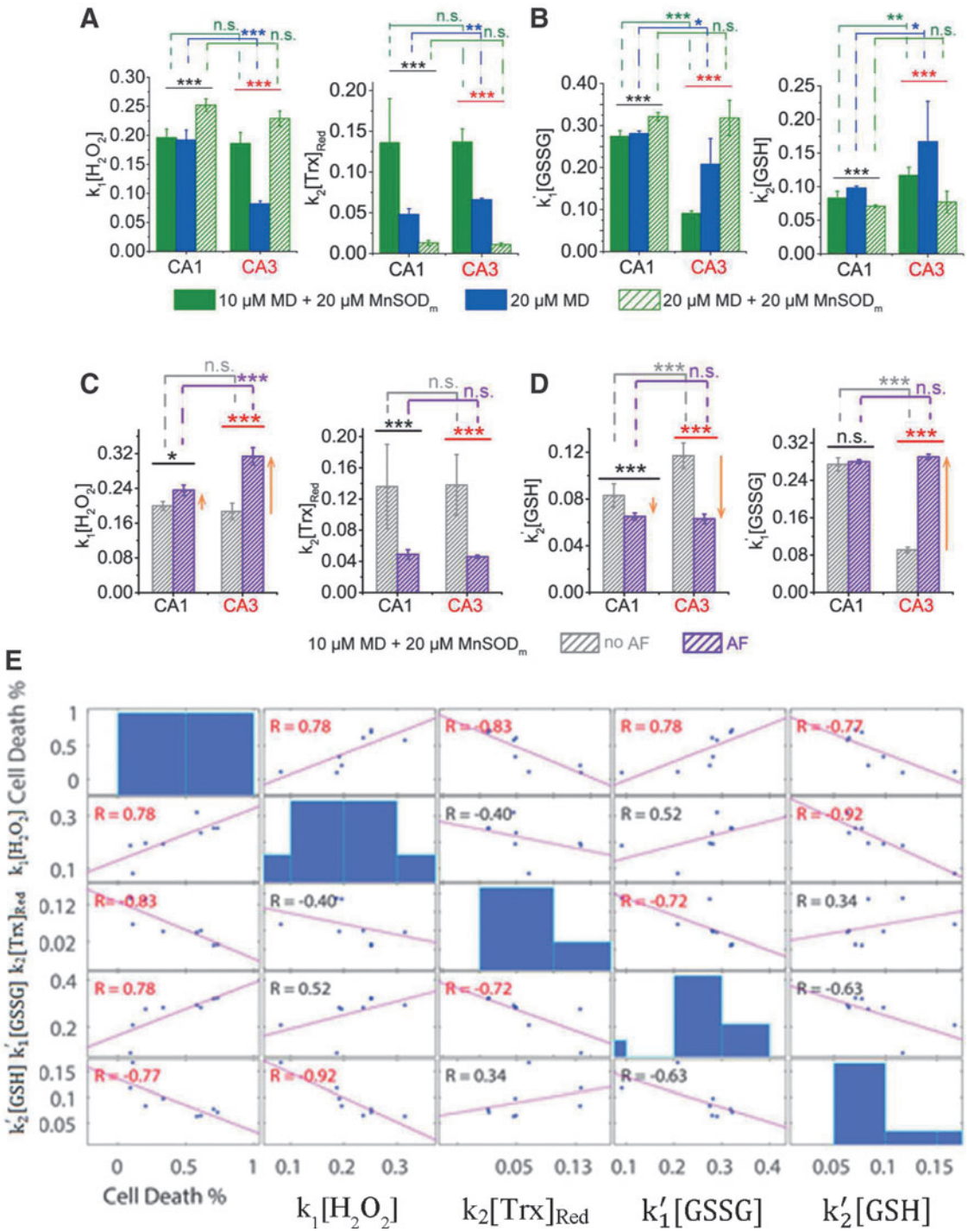

SUPPLEMENTARY FIG. S9. Rates from first-order exponential profiles of OxD_P and OxD_G and their correlations with each other and with cell death (related to Figs. 2–7). (A–D) Rates from exponential fits are represented as mean ± SEM ($n = 6$ repeats). See the Nonlinear Regression to the First-Order Exponential Equation section in Supplementary Data for more details. Statistical significance is marked as n.s., no significant difference/*$p < 0.05$/**$p < 0.01$/***$p < 0.001$. **(A, B)** Larger $k_1[H_2O_2]$ and $k_1'[GSSG]$ and smaller $k_2[Trx]_{Red}$ and $k_2'[GSH]$ demonstrate more oxidizing environment with increased [MD] or [$MnSOD_m$]. **(C, D)** AF enhances the oxidative stress induced by 10 μM MD +20 μM $MnSOD_m$. The difference of $k_2'[GSH]$ and $k_1'[GSSG]$ between CA1 and CA3 is abolished by AF. **(E)** $k_1[H_2O_2]$ and $k_1'[GSSG]$ are positively correlated with cell death, while $k_2[Trx]_{Red}$ and $k_2'[GSH]$ are negatively correlated with cell death. Negative correlation is also found between $k_2'[GSH]$ and $k_1[H_2O_2]$ and between $k_2[Trx]_{Red}$ and $k_1'[GSSG]$. Pearson's correlation coefficient is noted at each subplot and highlighted in *red* when $p < 0.05$ indicating the correlation is significant. All conditions of ±AF, ±MD, and ±$MnSOD_m$ from (A–D) are included.

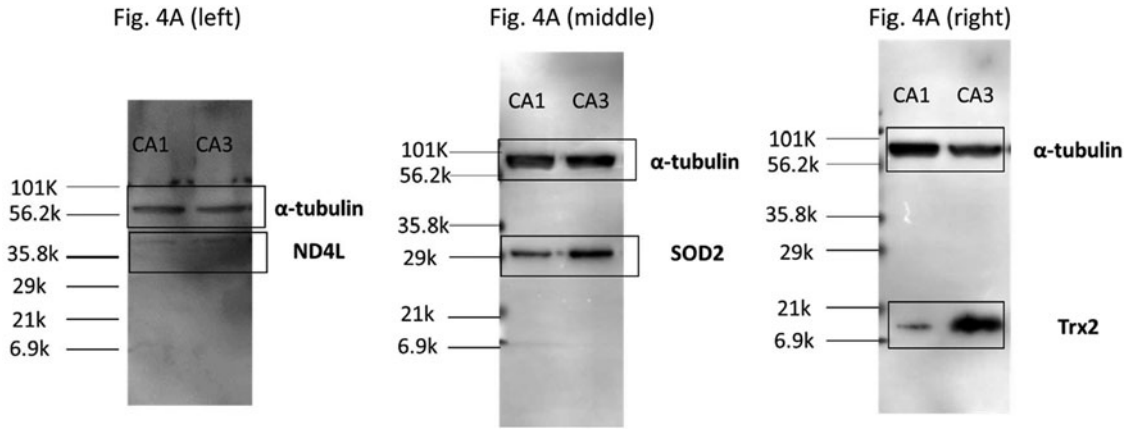

SUPPLEMENTARY FIG. S10. Uncropped blot for Western Blot data in Figure 4A. The full blots for ND4L, SOD2, and Trx2 are shown from *left* to *right* as the order in Figure 4.

SUPPLEMENTARY TABLE S1. DATA OF STEADY OXD FOR OXYGEN–GLUCOSE DEPRIVATION–REPERFUSION IN FIGURE 1E

	Basal	*OGD*	*RP*
OxD_P (mean ± SEM)			
Mito CA1	0.347 ± 0.018	0.250 ± 0.039	0.423 ± 0.028
Mito CA3	0.240 ± 0.090	0.269 ± 0.045	0.315 ± 0.054
Cyto CA1	0.266 ± 0.0274	0.342 ± 0.044	0.186 ± 0.023
Cyto CA3	0.260 ± 0.038	0.260 ± 0.037	0.200 ± 0.019
OxD_G (mean ± SEM)			
Mito CA1	0.295 ± 0.020	0.137 ± 0.026	0.489 ± 0.020
Mito CA3	0.317 ± 0.073	0.120 ± 0.031	0.241 ± 0.035
Cyto CA1	0.234 ± 0.038	0.157 ± 0.028	0.191 ± 0.023
Cyto CA3	0.302 ± 0.075	0.110 ± 0.031	0.227 ± 0.036

OGD, oxygen–glucose deprivation; RP, reperfusion.

Supplementary Table S2. Parameters of Peak of NAD(P)H for Oxygen–Glucose Deprivation–Reperfusion in Supplementary Figure S3

Peak parameters	*Peak 1*	*Peak 2*	*Peak 3*
Emerging time (min)	7.41 ± 0.52	11.7 ± 0.80	6.34 ± 0.36
Peak altitude (NFI)	1.07 ± 0.01	1.11 ± 0.01	1.10 ± 0.02
Ascending slope (NFI/min)	10.69 ± 2.08 ($\times 10^{-3}$)	20.2 ± 3.7 ($\times 10^{-3}$)	12.2 ± 3.7 ($\times 10^{-3}$)
Descending slope (NFI/min)	-5.26 ± 3.21 ($\times 10^{-3}$)	-12.5 ± 1.79 ($\times 10^{-3}$)	4.71 ± 1.33 ($\times 10^{-3}$)

NFI, normalized fluorescent intensity of NAD(P)H.

Supplementary Table S3. Data of OxD in Figure 2B (I–III) and D (I–III)

OxD (mean ± SEM)	*(I) basal*	*(II) 10 μM MD*	*(III) WO*
OxD_P CA1	0.078 ± 0.032	0.079 ± 0.018	0.077 ± 0.010
OxD_P CA3	0.072 ± 0.036	0.081 ± 0.021	0.073 ± 0.007
OxD_G CA1	0.104 ± 0.020	0.115 ± 0.025	0.106 ± 0.036
OxD_G CA3	0.091 ± 0.037	0.095 ± 0.021	0.095 ± 0.023

WO, washout.

Supplementary Table S4. Rates Fitted from Data of Figure 2B (IV), C (II, IV), D (IV), E (II), and E (IV) (Related to Supplementary Fig. S9A, B)

	CA1			*CA3*		
Fitting from OxD_P	$k_1[H_2O_2]$	$k_2[Trx]_{Red}$	OxD_{0P}	$k_1[H_2O_2]$	$k_2[Trx]_{Red}$	OxD_{0P}
10 μM MD +20 μM $MnSOD_m$	0.196 ± 0.015	0.136 ± 0.054	0.069 ± 0.047	0.186 ± 0.019	0.137 ± 0.016	0.085 ± 0.067
20 μM MD	0.192 ± 0.017	0.048 ± 0.007	0.073 ± 0.012	0.082 ± 0.001	0.066 ± 0.001	0.103 ± 0.054
20 μM MD +20 μM $MnSOD_m$	0.252 ± 0.011	0.013 ± 0.003	0.103 ± 0.045	0.252 ± 0.011	0.011 ± 0.002	0.103 ± 0.045
	CA1			*CA3*		
Fitting from OxD_G	$k_1'[GSSG]$	$k_2'[GSH]$	OxD_{0G}	$k_1'[GSSG]$	$k_2'[GSH]$	OxD_{0G}
10 μM MD +20 μM $MnSOD_m$	0.274 ± 0.014	0.083 ± 0.010	0.083 ± 0.016	0.091 ± 0.006	0.117 ± 0.012	0.109 ± 0.006
20 μM MD	0.281 ± 0.006	0.098 ± 0.003	0.103 ± 0.012	0.208 ± 0.061	0.167 ± 0.060	0.093 ± 0.054
20 μM MD +20 μM $MnSOD_m$	0.321 ± 0.010	0.071 ± 0.002	0.101 ± 0.080	0.318 ± 0.042	0.077 ± 0.016	0.099 ± 0.076

Supplementary Table S5. Rates Fitted from Data of Figure 5 (Related to Supplementary Fig. S9C, D)

	CA1			*CA3*		
Fitting from OxD_P	$k_1[H_2O_2]$	$k_2[Trx]_{Red}$	OxD_{0P}	$k_1[H_2O_2]$	$k_2[Trx]_{Red}$	OxD_{0P}
No AF	0.200 ± 0.010	0.136 ± 0.054	0.069 ± 0.047	0.187 ± 0.019	0.138 ± 0.039	0.085 ± 0.067
AF	0.236 ± 0.012	0.049 ± 0.006	0.109 ± 0.024	0.314 ± 0.02	0.046 ± 0.001	0.106 ± 0.015
	CA1			*CA3*		
Fitting from OxD_G	$k_1'[GSSG]$	$k_2'[GSH]$	OxD_{0G}	$k_1'[GSSG]$	$k_2'[GSH]$	OxD_{0G}
No AF	0.274 ± 0.014	0.083 ± 0.010	0.083 ± 0.016	0.091 ± 0.006	0.117 ± 0.011	0.109 ± 0.006
AF	0.280 ± 0.004	0.065 ± 0.003	0.081 ± 0.015	0.290 ± 0.006	0.063 ± 0.004	0.106 ± 0.008

Supplementary Table S6. Data of Steady OxD in Figure 6 for Oxygen–Glucose Deprivation–Reperfusion (Related to Supplementary Fig. S6)

		Basal	*OGD*	*RP*
OxD_P (mean ± SEM)				
Mito CA1	No AF	0.347 ± 0.018	0.250 ± 0.039	0.423 ± 0.028
	AF	0.321 ± 0.045	0.217 ± 0.033	0.485 ± 0.018
Mito CA3	No AF	0.240 ± 0.090	0.269 ± 0.045	0.315 ± 0.054
	AF	0.275 ± 0.063	0.279 ± 0.050	0.486 ± 0.057
OxD_G (mean ± SEM)				
Mito CA1	No AF	0.295 ± 0.020	0.137 ± 0.026	0.489 ± 0.020
	AF	0.392 ± 0.156	0.186 ± 0.060	0.607 ± 0.053
Mito CA3	No AF	0.317 ± 0.073	0.120 ± 0.031	0.241 ± 0.035
	AF	0.410 ± 0.101	0.198 ± 0.79	0.580 ± 0.076
OxD_P (mean ± SEM)				
Cyto CA1	No AF	0.150 ± 0.072	0.149 ± 0.076	0.169 ± 0.079
	AF	0.142 ± 0.014	0.195 ± 0.079	0.751 ± 0.071
Cyto CA3	No AF	0.171 ± 0.064	0.136 ± 0.082	0.145 ± 0.049
	AF	0.156 ± 0.024	0.233 ± 0.058	0.706 ± 0.060
OxD_G (mean ± SEM)				
Cyto CA1	No AF	0.116 ± 0.087	0.088 ± 0.036	0.098 ± 0.043
	AF	0.128 ± 0.042	0.158 ± 0.043	0.639 ± 0.039
Cyto CA3	No AF	0.154 ± 0.093	0.110 ± 0.064	0.099 ± 0.069
	AF	0.115 ± 0.021	0.153 ± 0.047	0.677 ± 0.022